Visualization of superposition states and Raman processes with two-dimensional atomic deflection

Gor A. Abovyan,[1,2,*] Gagik P. Djotyan,[3,†] and Gagik Yu. Kryuchkyan[1,2,‡]
[1]*Yerevan State University, A. Manookyan 1, AM-0025 Yerevan, Armenia*
[2]*Institute for Physical Research, Ashtarak-2, AM-0203 Ashtarak, Armenia*
[3]*Institute for Particle and Nuclear Physics of the Hungarian Academy of Sciences, Konkoly-Thege Miklós út 29-33, HU-1121 Budapest, Hungary*
(Received 15 November 2011; published 30 January 2012)

The deflection of atoms in a Λ-type configuration passing through two crossed standing light waves is proposed for the probing and visualization of atomic superposition states. For this goal, we use both the large-dispersive and Raman-resonant regimes of atom-field interaction, giving rise to position-dependent phase shifts of fields, and perform double simultaneous spatial measurements on an atom. In this way, it is demonstrated that the deflection spatial patterns of atoms in a Λ-configuration passing through modes of standing waves are essentially modified if the atoms are initially prepared in coherent superpositions of their low-level states as well as when the superposition states are created during the process of deflection. There are similar results for the joint momentum distributions of atoms. Furthermore, considering both one-photon- and two-photon-excitation regimes of Λ atoms, we also illustrate that the two-dimensional patterns of defected atoms qualitatively reflect the efficiency of the Raman processes.

DOI: 10.1103/PhysRevA.85.013846 PACS number(s): 37.30.+i, 42.50.Pq, 42.50.Dv, 42.50.St

I. INTRODUCTION

The ability to prepare atomic systems in superposition states is important both in fundamental studies of quantum mechanics as well as for various technological applications, including the fields of quantum information and quantum lithography. It is evident that the application of strong, near-resonant-to-atomic-transition laser light may result in the production and probing of the coherent superpositions of atomic and/or molecular states. In this way, many experiments have been proposed and realized, particularly with single trapped ions [1] and microwave-cavity quantum electrodynamics [2] with a single Rydberg atom coupled to a single field mode. The creation of such quantum states has also been realized for molecular systems [3], including large organic molecules [4]; for atomic ensembles [5]; and even for viruses [6]. Preparation of the atoms or molecules in the coherent superposition states may lead to substantial changes in optical properties of a medium composed of the particles. Some of the most spectacular examples are electromagnetically induced transparency with extreme changes in the group velocity of laser pulses, even including complete stopping of laser pulses (see Refs. [7,8]); enhancement of the efficiency of nonlinear optical processes [9,10]; and writing and storage of optical information in meta-stable quantum states [11–13]. The preparation of quantum coherence has also become of paramount importance for the growing field of quantum information science [14–16]. There exist some techniques for probing quantum interference based on the interaction of an atom in a superposition state with field modes. In this way, a final detection is realized by the homodyne measurement of states of a light field after its interaction with an atomic system as well as by the methods of quantum tomography [17]. Particularly, much work has been focused on the applications and developments of the technique of quantum tomography for atomic beams (see Ref. [18] and references therein).

One of the basic processes of atom optics is the deflection of atomic beams when interacting with a standing light wave inside an optical cavity. In this paper we demonstrate that production of atomic superposition states is qualitatively displayed in two-dimensional (2D) patterns of deflected atoms on two crossed standing waves. The analysis is done in quantum treatment for three-level atoms in a Λ configuration, interacting with two crossed standing light waves. We demonstrate that the deflection patterns of the atomic beam passing through two crossed standing light waves are modified if the atoms are initially prepared in coherent superpositions of the lower-level states or as well as when the superposition states are created during the process of deflection. Our other goal is to understand how Raman processes under the general two-photon-resonance condition are exhibited in the atomic deflection patterns. Considering different interaction regimes of a Λ system with off-resonant standing waves, we have demonstrated that the deflection patterns, in the transverse plane to the direction of the center-of-atomic-mass motion, are essentially different for the cases of one-photon and two-photon Raman interactions.

The approach proposed relies on the problem of atomic spatial localization. In general, the precise spatial measurements and localizations of quantum particles have been a subject of considerable interest since the discussion of Heisenberg's famous microscope. A particular class of quantum-optical-localization schemes suitable to determine the position of a quantum particle on a subwavelength scale makes use of standing-wave driving fields (see Refs. [19–26]).

It is well known that when atoms pass a standing-wave cavity mode, the strength of interaction with a field depends on the positions of the atoms. Thus, quadrature-phase measurements of the field lead to strong localization of the atomic position below the wavelength of the field in the

*gor.abovyan@ysu.am
†djotjan@rmki.kfki.hu
‡kryuchkyan@ysu.am

cavity [19,20]. Recently, atomic-localization and center-of-mass wave-function measurements via multiple simultaneous dispersive interactions of atoms with different standing-wave fields have been investigated [27] in addition to the well-known results for a single-mode cavity [19–26]. Note that the analogous scheme of atomic deflection has been recently considered for the investigation of spatial entanglement in the deflection of V-type atoms [28,29] as well as Λ-type atoms [30]. Thus, we apply the measurement-induced-localization procedure for our scheme, calculating the conditional position distribution of atoms while considering the two-mode field to be in a given reference quadrature-phase state. As it will be shown here, for narrow initial position distributions of atoms, our scheme permits producing controllable pattern structures with feature spacing smaller than the wavelength of the light in the cavity.

For completeness, we also discuss the visualization of atomic superposition states in the momentum space. In this vein, the distribution of deflected atoms in terms of the transverse atomic moment is calculated. It is evident that for narrow initial atomic wave packets, wider distributions in the momentum space will be realized.

This paper is organized as follows. In Sec. II we introduce the system and obtain the formulas for the conditional position distribution of atoms. In Sec. III we present the results for the probing of superposition states for both schemes of measurement—near the cavity zones and outside the cavity in far-diffraction zones. The momentum distributions are also calculated. Section IV is devoted to visualization of the Raman resonance. Section V concludes the paper.

II. ATOMIC DEFLECTION IN THE PRESENCE OF TWO-PHOTON RAMAN PROCESSES

Let us consider the quantum dynamics of a three-level atom with a Λ-type configuration of energy levels moving along the z direction and passing through cavities that involve two crossed one-mode standing waves (see Fig. 1). The atomic beam is adjusted so that only one atom interacts with the cavity's electromagnetic field at a time, and the position patterns of the deflected atoms in the xy plane are measured. The transition between the two lower levels $|1\rangle$ and $|2\rangle$ is dipole forbidden, and the transitions from the upper level $|3\rangle$ to either of the lower levels $|1\rangle$ or $|2\rangle$ are allowed. We focus more specifically on the dispersive limit at which

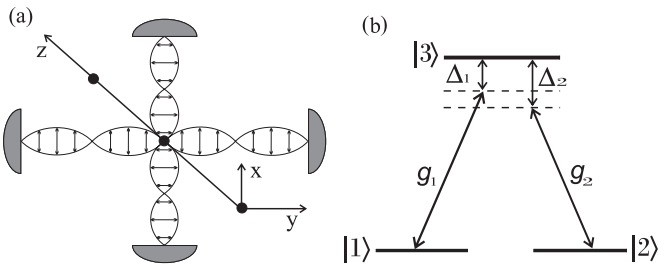

FIG. 1. Schematic diagrams showing the investigated model. (a) The atomic beam crossing the interaction region. (b) Energetic levels of a Λ-type atom with equal energies of the sublevels interacting with modes of opposite circular polarizations with coupling constants g_1 and g_2.

the detuning between the two standing-wave frequencies and the corresponding atomic-transition frequencies are large compared with the Rabi frequencies. We also neglect the atomic damping during the time an atom interacts with the fields.

We consider two standard types of Hamiltonian depending on two detunings Δ_1 and Δ_2. If the frequencies of the modes and the duration τ of the atom-field interaction are adjusted so that $\Delta_1 - \Delta_2 \ll \pi/\tau$, the case of two-photon resonance $\Delta_1 = \Delta_2 = \Delta$ can be realized with the following effective Hamiltonian

$$H_{\rm eff} = \sum_{i=1,2} \frac{\hbar g_i^2}{\Delta} a_i^\dagger a_i \sigma_{ii} + \frac{\hbar g_1 g_2}{\Delta}(a_1^\dagger a_2 \sigma_{12} + a_1 a_2^\dagger \sigma_{21}). \quad (1)$$

Here a_i and $a_i^\dagger$ are the annihilation and creation operators of the ith mode, respectively, while $\sigma_{ij} = |i\rangle\langle j|$ is the corresponding transition operator of the Λ atom. The couplings of the atom to the two modes are determined by the spatial-mode functions $g_1(x) = g_{01}\sin(k_1 x)$ and $g_2(y) = g_{02}\sin(k_2 y)$, where $g_{0i} = E_0 \vec{e}_i \langle i|\vec{d}|3\rangle$, $i = 1,2$, and k_i is the wave vector of the ith mode. E_0 is the so-called electric field per photon. $\vec{e}_1$ and $\vec{e}_2$ are the polarization vectors while $\langle 1|\vec{d}|3\rangle$ and $\langle 2|\vec{d}|3\rangle$ are the dipole moments of the corresponding atomic transitions. The last term in the expression (1) describes the connection between the two interaction channels due to two-photon (Raman) transitions between the $|1\rangle$ and $|2\rangle$ levels. When the condition of the Raman resonance is not carried out and the contributions of the Raman transitions may be neglected, the interaction Hamiltonian reads as

$$H_{\rm eff} = \sum_{i=1,2} \frac{\hbar g_i^2}{\Delta_i} a_i^\dagger a_i \sigma_{ii}. \quad (2)$$

The initial position distribution of atoms at the entrance of a cavity is assumed to be Gaussian, i.e.,

$$|f(x,y)|^2 = \frac{1}{2\pi\,\Delta x \Delta y} e^{-\frac{(x-\langle x\rangle)^2}{2(\Delta x)^2}} e^{-\frac{(y-\langle y\rangle)^2}{2(\Delta y)^2}} \quad (3)$$

with the widths $\Delta x = \sqrt{\langle (x-\langle x\rangle)^2\rangle}$ and $\Delta y = \sqrt{\langle (y-\langle y\rangle)^2\rangle}$ centered at the nodes of both waves while the initial atomic states are considered in general as $a|1\rangle + b|2\rangle$ with a and b being the weights of the atomic lower states in the coherent superposition. The cavity modes are assumed to be initially in a two-mode coherent state

$$|\text{field}\rangle = |\alpha_1\rangle_1 |\alpha_2\rangle_2, \quad |\alpha\rangle_i = e^{-N/2} \sum_n \frac{\alpha^n}{\sqrt{n!}} |n\rangle_i, \quad (4)$$

where $|n\rangle_i$ are the Fock states for the ith mode and $N = |\alpha|^2$. In this case, the state vector of this system at time t will have the form

$$|\Psi(t)\rangle = \int dx dy \sum_{i=1,2} \sum_{n,m=0}^{\infty} \Phi_{n,m}^{(i)}(x,y,t)|n\rangle_1 |m\rangle_2 |i\rangle |x,y\rangle, \quad (5)$$

where the amplitudes $\Phi_{n,m}^{(i)}(x,y,t)$ can be derived from the following equation and its corresponding initial conditions

$$i\hbar \frac{\partial}{\partial t}|\Psi(t)\rangle = \hat{H}_{\rm eff}|\Psi(t)\rangle,$$

$$|\Psi(t=0)\rangle = \int dxdyf(x,y)|x,y\rangle \otimes(a|1\rangle + b|2\rangle) \otimes |\alpha_1\rangle_1|\alpha_2\rangle_2, \quad (6)$$

by substituting $|\Psi(t)\rangle$ in Eq. (6) with the expression (5). In the case of two-photon resonance, the amplitudes are written as

$$\Phi^{(1)}_{n,m}(x,y,t) = f(x,y)\left\{aC_{n,m} + G_1\left[\exp\left(-\frac{it}{\Delta}\Omega_{n,m+1}\right) - 1\right]\right\}, \quad (7a)$$

$$\Phi^{(2)}_{n,m}(x,y,t) = f(x,y)\left\{bC_{n,m} + G_2\left[\exp\left(-\frac{it}{\Delta}\Omega_{n+1,m}\right) - 1\right]\right\}, \quad (7b)$$

where

$$G_1 = \frac{g_1g_2\sqrt{n(m+1)}}{\Omega_{n,m+1}}C_{n-1,m+1}b + \frac{g_1^2n}{\Omega_{n,m+1}}C_{n,m}a, \quad (8a)$$

$$G_2 = \frac{g_1g_2\sqrt{(n+1)m}}{\Omega_{n+1,m}}C_{n+1,m-1}a + \frac{g_2^2m}{\Omega_{n+1,m}}C_{n,m}b, \quad (8b)$$

where $\Omega_{n,m} = g_1^2n + g_2^2m$ is the position-dependent Rabi frequency and

$$C_{n,m} = e^{-(|\alpha_1|^2+|\alpha_2|^2)/2}\left(\frac{\alpha_1^n\alpha_2^m}{\sqrt{n!m!}}\right). \quad (9)$$

The functions $\Phi^{(i)}_{n,m}(x,y,t)$ describe the amplitude distributions for the positions of atoms in the xy plane. They are proportional to the atomic-initial-position distribution and also display nontrivial spatial features due to position-dependent phase shifts acquired by Λ atoms passing through standing waves.

It is well known [18,19] that the measurement of the phase shift of the cavity fields can be interpreted as a quantum spatial localization of the atom. In this way, below we investigate the deflection of atoms with simultaneous quadrature measurements of the field. We have studied this problem in details for one-dimensional atomic deflection as well as for the two-dimensional case in the dispersive limit, assuming a negligibly small contribution of the Raman transitions in the system. In this case, there is no exchange of energy between the field and the atom, i.e., the interaction does not change the internal atomic state. This situation is cardinally changed for the Λ atom under the two-photon-resonance condition. Indeed, in this case both amplitudes, $\Phi^{(1)}_{n,m}(x,y,t)$ and $\Phi^{(2)}_{n,m}(x,y,t)$, corresponding to the two atomic states $|1\rangle$ and $|2\rangle$, govern the spatial distribution of deflected Λ atoms. Thus, the interaction between the atom and the intracavity field beside the initial position of the atom depends also on its internal states. The latter allows visualization of the atomic coherence in the final position distribution of the atom.

III. PROBING AND VISUALIZATION OF THE ATOMIC COHERENCE BY THE DEFLECTION PATTERNS

A. Position distributions

In this section, we focus on studies of position distributions assuming that the cavity modes are in a given reference state. Two schemes of joint measurements have been proposed up to now, based on quadrature measurements of standing-wave fields as well as on measurements of the phase states [18,19]. We start by considering the case of the quadrature measurement; the other case will be considered in Sec. IV. To realize this we consider implementation of a quadrature measurement on the field and use the following expression for the field quadrature state:

$$|\chi_\theta\rangle = (2\pi)^{-1/4}e^{[-(a^\dagger e^{i\theta}-\chi_\theta)^2/2+\chi_\theta^2/4]}|\text{vac}\rangle. \quad (10)$$

Here, parameter θ is an angle characterizing the one-mode field quadrature in the Wigner plane, χ_θ is the corresponding eigenvalue, and $|\text{vac}\rangle$ denotes the vacuum state with zero photons in the cavity. Here, we are interested in the calculation of the probability of finding an atom at position (x,y) provided that a measurement of the two field modes with angles θ_1 and θ_2 is performed. Using the reference state as $|\chi_{\theta_1}\rangle_1|\chi_{\theta_2}\rangle_2$, where the quadrature state $|\chi_{\theta_i}\rangle_i$ corresponds to the operator a_i, we obtain the joint probability as

$$W(\chi_{\theta_1},\chi_{\theta_2},x,y) = \sum_{i=1,2}|_1\langle\chi_{\theta_1}|_2\langle\chi_{\theta_2}|\langle i|\langle x,y|\Psi(t)\rangle|^2 = \sum_{i=1,2}\left|\sum_{n,m=0}^{\infty}\Phi^{(i)}_{n,m}(x,y,t)_1\langle\chi_{\theta_1}|n\rangle_{12}\langle\chi_{\theta_2}|m\rangle_2\right|^2. \quad (11)$$

We obtain the general expression for the factor $\langle\chi_\theta|n\rangle$ using the formula (10). This matrix element can be calculated as follows:

$$\langle\chi_\theta|n\rangle = \frac{1}{\pi}\int\langle\chi_\theta|\alpha\rangle\langle\alpha|n\rangle d^2\alpha, \quad (12)$$

where

$$\langle\chi_\theta|\alpha\rangle = \frac{e^{-|\alpha|^2/2}}{(2\pi)^{1/4}}\left[e^{-(\alpha e^{-i\theta}-\chi_\theta)^2/2+\chi_\theta/4}\right] \quad (13)$$

and

$$\langle\alpha|n\rangle = e^{-|\alpha|^2/2}\frac{(\alpha^*)^n}{\sqrt{n!}}. \quad (14)$$

Similarly, the factors corresponding to the states $|\chi_{\theta_1}\rangle_1$ and $|\chi_{\theta_2}\rangle_2$ can be calculated.

In the following, we show how various initial atomic states in the form $a|1\rangle + b|2\rangle$, where $|a|^2 + |b|^2 = 1$, with definite quadrature measurements can change the joint probability. Some typical results are depicted in Fig. 2 as 2D distributions for the various superposition states $a|1\rangle + b|2\rangle$ as well as for the joint probabilities in the 3D representation. The examples are taken for the measurement angles $\theta_1 = \theta_2 = 0$, $\alpha_1 = \alpha_2 = 2$, $\chi_{\theta_1} = \chi_{\theta_2} = 4$, and $\Delta x = \Delta y = 0.2\lambda_1$, where $\lambda_1 = 2\pi/k_1$. Considering the 2D position distributions at the fixed parameters $\theta_1 = \theta_2$ and $\alpha_1 = \alpha_2$, we conclude that the atomic distributions are turned in the xy plane around the center $x = y = 0$, depending on the coefficients a and b. The figures showing these features are presented in Figs. 2(a)–2(f).

As our analysis shows, the orientation of the distribution changes with the value of the fraction a/b when it is varying from $-\infty$ to ∞ and any given orientation corresponds to a particular value of a/b. In general, the fraction a/b is a complex number, and we can represent it as $(a/b)_{\text{real}}e^{i\varphi}$, where $\varphi \in (-\pi/2,\pi/2)$ and $(a/b)_{\text{real}} \in (-\infty,\infty)$. It turns out that

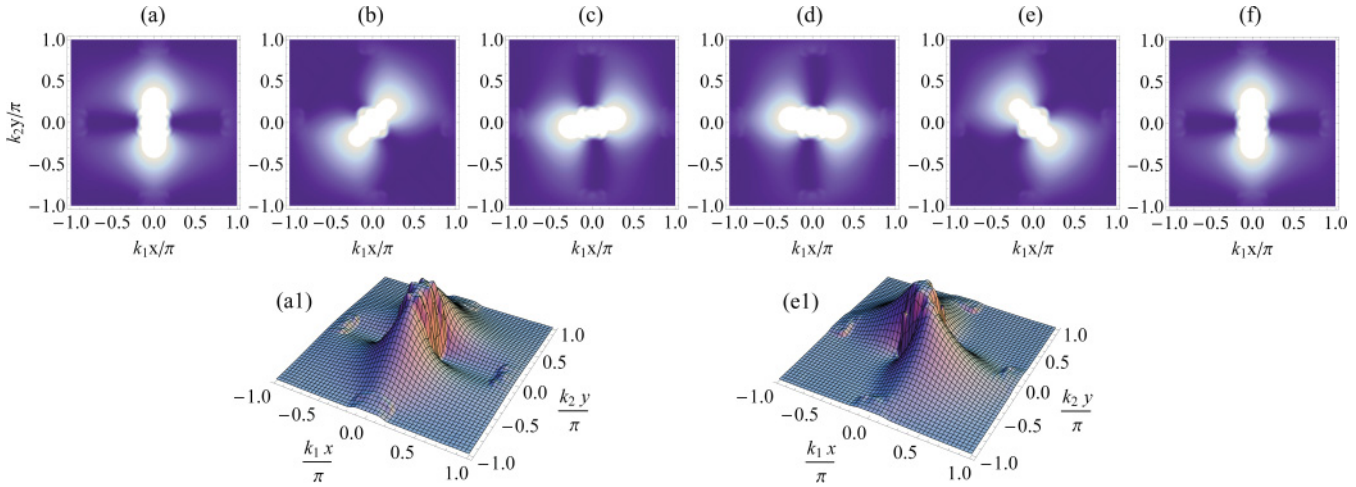

FIG. 2. (Color online) A set of diagrams showing the atomic distribution's circular dependence on the initial internal atomic state. Bright colors indicate high probability, and dark colors indicate low probability. The parameters are $\theta_1 = \theta_2 = 0$, $\alpha_1 = \alpha_2 = 2$, $\chi_{\theta_1} = \chi_{\theta_2} = 4$, $\Delta x = \Delta y = 0.2\lambda_1$, and $\lambda_1 = 2\pi/k_1$. (a) $a = -1$, $b = 0$; (b) $a = -1/\sqrt{2}$, $b = 1/\sqrt{2}$; (c) $a = -0.2$, $b = 0.98$; (d) $a = 0.2$, $b = 0.98$; (e) $a = 1/\sqrt{2}$, $b = 1/\sqrt{2}$; and (f) $a = 1$, $b = 0$. (a1) is the same as (a) in the 3D representation. (e1) is the same as (e) in the 3D representation.

the additional factor $e^{i\varphi}$ does not change the orientation of the spatial distribution but changes the level of its stretching in the direction of orientation. Thus, the distributions corresponding to $(a/b)_{\text{real}}$ and $(a/b)_{\text{real}}e^{i\varphi}$ are qualitatively the same. This fact provides the possibility to calculate the $(a/b)_{\text{real}}$ fraction from a given final-atomic-position distribution.

Thus, we demonstrate in Fig. 2 that the atomic superposition state can be qualitatively probed in two-dimensional patterns of deflected atoms. Indeed, the distribution corresponding to the superposition state $\frac{1}{\sqrt{2}}(|1\rangle + |2\rangle)$ [Fig. 2(e)] is turned on $\pi/4$ relative to the position distribution of Λ atoms that are initially in the state $|1\rangle$ [Figs. 2(a) and 2(f)].

As our analysis shows, for higher values of the parameters α_1 and α_2 than those that have been used in our example, the forms of the distributions are essentially the same. The slight differences are related to additional relatively small structures that do not change the spatial-orientation features of the distribution. Thus, obtained results are applicable also for more intensive electromagnetic fields. The choice of the particular values $\theta_1 = \theta_2 = 0$ of the parameters θ_1 and θ_2 are conditioned by the explicitness of the effects described above. The above results are mainly valid also for the other values of the measurement angles θ_1 and θ_2 although they differ in details from the results presented in Fig. 2.

B. Position distribution in the far-diffraction zone

For the completeness of our analysis, we added in this section calculations for the position distribution of atoms in the far-field-diffraction zone. This analysis is important for an experimental verification of the obtained effects. It allows us to consider the obtained effects for realistic experimental conditions and hence defining the spatial resolution necessary for the detection of these effects.

To modify previous calculations, we use the expression for the free Hamiltonian of atoms $H_{\text{free}} = \hat{p}^2/(2m)$ and rewrite the state vector of a system at time $t + t_0$, where t is the free propagation time, in the following form

$$|\Psi(t+t_0)\rangle = \exp\left(-\frac{i}{\hbar}H_{\text{free}}t\right)|\Psi(t_0)\rangle = \int dxdy \sum_{i=1,2}\sum_{n,m=0}^{\infty} \bar{\Phi}^{(i)}_{n,m}(x,y,t)|n\rangle_1|m\rangle_2|i\rangle|x,y\rangle, \tag{15}$$

where

$$\bar{\Phi}^{(i)}_{n,m}(x,y,t) = -\frac{iM}{2\pi\hbar t}\int dx'dy'\Phi^{(i)}_{n,m}(x',y',t_0) \times \exp\left\{\frac{iM}{2\hbar t}[(x-x')^2 + (y-y')^2]\right\}. \tag{16}$$

From Eq. (15), it is clear that for calculations of the position distribution in the far-field-diffraction zone, we can use the expression (11) just by replacing $\Phi^{(i)}_{n,m}(x,y,t)$ with $\bar{\Phi}^{(i)}_{n,m}(x,y,t)$. The results of the numerical calculations of the distributions for the near- and far-field regions are depicted in Fig. 3, which shows a slight difference between them. The distribution in Fig. 3(b) corresponds to the distance $L = vt = 50$ cm from the exit of the cavity at which v is the velocity of the atomic-mass center in the z direction, and for its value we have chosen 100 m/s.

C. Momentum distributions

The other approach analyzing the atomic deflection process concerns the momentum distributions of atoms. In this section, we shortly discuss the momentum distribution in the deflected patterns of the Gaussian atomic wave packet, assuming the width of the wave packet to be much smaller than the wavelength of the modes. We calculate the probability of finding an atom with the transverse momentum (p_x, p_y) provided that a measurement of the two field modes with angles θ_1 and θ_2 is performed. This procedure is similar to

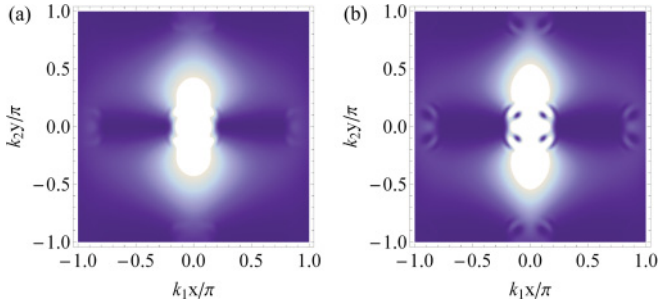

FIG. 3. (Color online) The position distribution $W(x,y)$ for $\Delta x = \Delta y = 0.2\lambda_1, \lambda_1 = 2\pi/k_1$, and the initial internal state of the atom $a = 1$ and $b = 0$. Brighter colors indicate higher values of the distribution. The distribution (a) at the exit of the cavity and (b) at a distance $L = vt = 50$ cm from the exit of the cavity.

the calculation of the conditional position distribution made above. Thus, the momentum distribution is written as

$$P(\chi_{\theta_1},\chi_{\theta_2},p_x,p_y) = \sum_{i=1,2} |{}_1\langle\chi_{\theta_1}|{}_2\langle\chi_{\theta_2}|\langle i|\langle p_x,p_y|\Psi(t)\rangle|^2 = \sum_{i=1,2}\left|\sum_{n,m=0}^{\infty}\tilde{\Phi}^{(i)}_{n,m}(p_x,p_y,t){}_1\langle\chi_{\theta_1}|n\rangle_1{}_2\langle\chi_{\theta_2}|m\rangle_2\right|^2, \quad (17)$$

where the amplitude in the momentum space is calculated by the Fourier transformation over the spatial variables

$$\tilde{\Phi}^{(i)}_{n,m}(p_x,p_y,t) = \frac{1}{2\pi}\int\int dxdy\Phi^{(i)}_{n,m}(x,y,t) \times \exp\left[-\frac{i}{\hbar}(p_x x + p_y y)\right]. \quad (18)$$

We illustrate the momentum distributions for narrow initial atomic wave packets, which obviously correspond to a wider distribution in the momentum space. As the analysis shows, in contrast to the position distributions, the dependence of the momentum distributions on initial internal states is not so evident, but in some cases it is still possible to find visible relations between the distribution and the initial internal state. The momentum distributions for two cases of initial atomic superposition states with the coefficients $a = -1/\sqrt{2}$ and $b = 1/\sqrt{2}$ and $a = 1/\sqrt{2}$ and $b = 1/\sqrt{2}$ are shown in Fig. 4. Comparing Figs. 4(a) and 4(b), we realize that the ranges of localizations of the momenta for these cases are stretched in perpendicular directions, i.e., the distribution corresponding to the superposition state $\frac{1}{\sqrt{2}}(|1\rangle + |2\rangle)$ is turned on $\pi/2$ relative to the momentum distribution of Λ atoms that are initially in the state $\frac{1}{\sqrt{2}}(|1\rangle - |2\rangle)$. Comparing the results of the momentum distributions with the corresponding position distributions in Figs. 2(b) and 2(e), we conclude that they are in accordance with uncertainty relations.

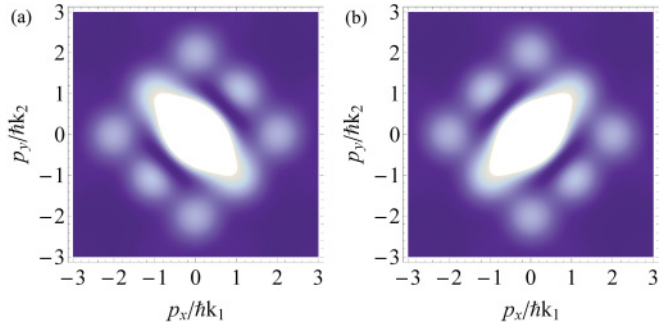

FIG. 4. (Color online) The momentum distribution $P(p_x,p_y)$ for $\Delta x = \Delta y = 0.2\lambda_1$ and $\lambda_1 = 2\pi/k_1$. Brighter colors indicate higher values of the distribution. The initial internal states of the atom are (a) $a = -1/\sqrt{2}$, $b = 1/\sqrt{2}$ and (b) $a = 1/\sqrt{2}$, $b = 1/\sqrt{2}$. We use the dimensionless momenta scaled in units of $\hbar k$.

IV. EVIDENCE OF RAMAN RESONANCE IN ATOMIC DEFLECTION

In this section we illustrate the principal differences between the cases of interaction in Raman resonance and ordinary off-resonance from the point of view of an atomic-beam deflection by two crossed standing waves. In this way, we derive the amplitudes $\Phi^{(i)}_{n,m}(x,y,t)$ in Eq. (5) for the interaction Hamiltonian (2). For the atomic initial internal state $a|1\rangle + b|2\rangle$, the amplitudes are written as

$$\Phi^{(1)}_{n,m}(x,y,t) = f(x,y)C_{n,m}\exp\left(-i\frac{g_1^2 t}{\Delta_1}n\right)a, \quad (19a)$$

$$\Phi^{(2)}_{n,m}(x,y,t) = f(x,y)C_{n,m}\exp\left(-i\frac{g_2^2 t}{\Delta_2}m\right)b. \quad (19b)$$

Considering different regimes of interaction of the Λ atom by using the spatial amplitudes of Eqs. (7), (8), and (19), we demonstrate that the deflection patterns are essentially different for the cases of one-photon and two-photon interaction. The most convenient approach to realize our goal is the investigation of the conditional position distribution of atoms, provided that the two-mode field is in a given phase state

$$|\Psi_R\rangle = |\varphi_1\rangle_1|\varphi_2\rangle_2, \quad (20)$$

where

$$|\varphi\rangle_i = \frac{1}{\sqrt{2\pi}}\sum_n e^{-i\varphi n}|n\rangle_i. \quad (21)$$

The discussed distribution is

$$W(x,y) = \sum_{i=1,2}|\langle x,y|\langle i|\langle\Psi_R|\Psi(t)\rangle|^2. \quad (22)$$

Using the formulas (5) and (19)–(22), we obtain the following expression for $W(x,y)$:

$$W(x,y) = \frac{1}{(2\pi)^2}\sum_{i=1,2}\left|\sum_{n,m}\Phi^{(i)}_{n,m}(x,y,t)e^{-i(n\varphi_1+m\varphi_2)}\right|^2. \quad (23)$$

Obviously, distributions (19) and (23) crucially depend on phases φ_1 and φ_2, which concretize the ranges of atom-wave interactions. We choose $\varphi = 0$, which gives the best spatial localization of the scattered atoms. Thus, the probability $W(x,y,\varphi = 0) = W(x,y)$ describes the selected scattering events of only those atoms that have passed the nodes of the field with the spatial-mode functions $\sin(k_1x)$ and $\sin(k_2y)$. As it was shown earlier, such a joint measurement procedure plays the role of a spatial filter. Experimentally, this procedure can be realized by a mechanical slit or mask placed in front of

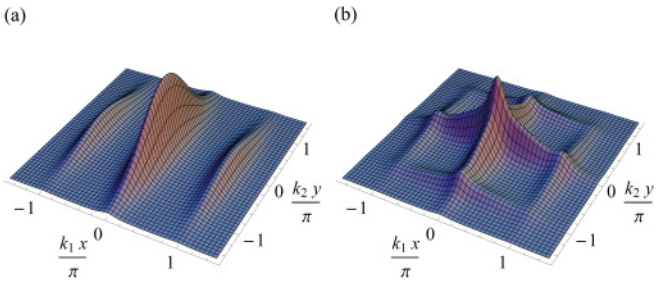

FIG. 5. (Color online) The position distribution function $W(x,y)$ for the case of $\Delta_1 \neq \Delta_2$, $\Delta x = \Delta y = 0.3\lambda_1$, and $\lambda_1 = 2\pi/k_1$. The initial state of the atom is described by (a) $a = 1$, $b = 0$ and (b) $a = 1/\sqrt{2}$, $b = 1/\sqrt{2}$.

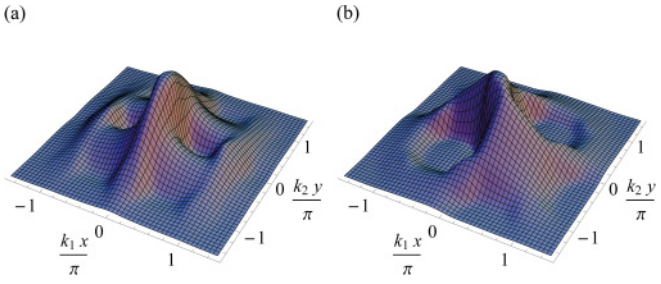

FIG. 6. (Color online) The position distribution function $W(x,y)$ for the case of $\Delta_1 = \Delta_2$, $\Delta x = \Delta y = 0.3\lambda_1$, and $\lambda_1 = 2\pi/k_1$. The initial state of the atom is described by (a) $a = 1$, $b = 0$ and (b) $a = 1/\sqrt{2}$, $b = 1/\sqrt{2}$.

a node of the electromagnetic field. For a detailed discussion of this point, see Ref. [18].

The results of concrete calculations based on Eq. (23) are depicted in Figs. 5 and 6 for the different regimes of interaction. In Fig. 6 the position-distribution functions $W(x,y)$ are depicted in the case of two-photon resonant interaction and for two different choices of the initial coherence of the internal atomic state. As we can see, these results are similar to those in Figs. 2(a1) and 2(e1) obtained for the quadrature-measurement scheme. The case of different detunings leading to one-photon atomic transitions is depicted in Fig. 5. Comparing two types of the graphics allows us to make clear the peculiarities of coherent Raman processes in comparison with corresponding one-photon processes from the point of view of atomic optics.

Let us consider the probability distributions depicted in Figs. 5(a) and 6(a) that correspond to the situation when atoms enter the cavity being initially in the lower state $|1\rangle$. As we see, the position distribution in Fig. 5(a) shows a high spatial localization of deflected atoms in the x direction while in the y direction their behavior has remained unchanged, i.e., determined by the initial Gaussian distribution. In other words, the impact of the initial field state is the one-dimensional distribution of the atoms. It could be anticipated because in this case the atom and the field interact through only one channel (the interaction between the first mode of the field and the $|1\rangle \leftrightarrow |3\rangle$ transition) as the atom, due to the off-resonant nature of the interaction, always remains in the state $|1\rangle$. In contrast to this, in the case of two-photon resonance, the two-photon $|1\rangle \leftrightarrow |2\rangle$ transition leads to the activation of the interaction between the second mode of the field and the $|2\rangle \leftrightarrow |3\rangle$ transition. As a result, the structure of the position distribution in Fig. 6(a) has acquired some features indicating this fact. The distribution showing the localization near some points in both the x and y directions is described by two-dimensional patterns. Particularly, it is expressed by the emergence of four additional walls forming a structure resembling two closed cycles [see Fig. 6(a)].

If the atom enters the cavity in a superposition of two lower $|1\rangle$ and $|2\rangle$ states, the impact of the field on the atomic position distributions contains two-dimensional localization patterns even in the case of the absence of Raman transitions [see Figs. 5(b) and 6(b)]. The difference between the distributions of the two considered regimes becomes obvious when we analyze the graphics in the following manner. If Raman resonance is violated, the position distribution [see Fig. 5(b)] is described by two perpendicular planes of symmetry passing through the x and y axes. It expresses the fact that the impact of the interaction between the first mode and the $|1\rangle \leftrightarrow |3\rangle$ transition and the impact of the interaction between the second mode and the $|2\rangle \leftrightarrow |3\rangle$ transition are independent. They depend only on the populations in the corresponding atomic levels, which in this regime at the beginning of the interaction are equal to $|a|^2$ and $|b|^2$, respectively [see Eq. (1)]. In the two-photon-resonance regime, the $|1\rangle \leftrightarrow |2\rangle$ transition destroys this independence and, hence, leads to the breaking of the symmetry. This fact is evidently reflected in Fig. 6(b) in which x and y are not axes of symmetry for the distribution.

V. SUMMARY

By calculating the concrete conditional spatial distributions of Λ-structured atoms after passing two crossed standing light waves, we have shown that two-dimensional patterns of deflected atoms contain important information concerning the low-level atomic superposition states as well as reflect the efficiency of the two-photon resonant Raman process. Thus, we have developed an approach for the testing and visualization of superposition states as well as for probing the Raman resonance in a new nonspectroscopic manner. In more detail, we have studied how various initial atomic superposition states $a|1\rangle + b|2\rangle$ in the Gaussian atomic beam are visualized in both 2D and 3D distributions of the joint probabilities. In this way, we have demonstrated that at fixed values of the parameters $\theta_1 = \theta_2$ and $\alpha_1 = \alpha_2$, the atomic spatial patterns are turned in the xy plane around the center $x = y = 0$ on an angle depending on the values of the coefficients a and b describing the weights of the atomic-lower-state probabilities in the initial superposition state. This analysis has been done for both near- and far-field-diffraction zones as well as in the momentum space. Considering two regimes of the interaction of Λ-type atoms with a two-mode field, we have clearly demonstrated with the spatial patterns the peculiarities of coherent Raman processes in comparison with corresponding one-photon processes from the point of view of atomic optics.

ACKNOWLEDGMENTS

G.Yu.K. acknowledges helpful discussions with J. Evers, C. H. Keitel, M. Macovei, and M. Zubairy.

The authors acknowledge a collaboration grant from the Armenian and Hungarian Academies of Sciences. G.P.D. acknowledges the support of the Research Fund of the Hungarian Academy of Sciences (OTKA) under Contracts No. K 68240 and No. NN 78112 as well as the Grant No. ELI-09-1-2010-0010.

[1] C. Monroe, D. M. Meekhof, B. E. King, and D. J. Wineland, Science **272**, 1131 (1996); C. J. Myatt, Nature (London) **403**, 269 (2000).
[2] J. M. Raimond, M. Brune, and S. Haroche, Rev. Mod. Phys. **73**, 565 (2001).
[3] M. Arndt *et al.*, Nature (London) **401**, 680 (1999).
[4] S. Gerlich *et al.*, Nat. Commun. **2**, 263 (2011).
[5] C. J. Myatt *et al.*, Nature (London) **403**, 269 (2000).
[6] O. Romero-Isart, M. L. Juan, R. Quidant, and J. I. Cirac, New J. Phys. **12**, 033015 (2010).
[7] M. D. Lukin, Rev. Mod. Phys. **75**, 457 (2003).
[8] M. Fleischhauer, A. Imamoglu, and J. P. Marangos, Rev. Mod. Phys. **77**, 633 (2005).
[9] M. Jain, H. Xia, G. Y. Yin, A. J. Merriam, and S. E. Harris, Phys. Rev. Lett. **77**, 4326 (1996).
[10] M. D. Lukin, P. R. Hemmer, M. Loffler, and M. O. Scully, Phys. Rev. Lett. **81**, 2675 (1998).
[11] G. P. Djotyan, J. S. Bakos, and Z. Sorlei, Opt. Express **4**, 113 (1999).
[12] G. P. Djotyan, J. S. Bakos, and Z. Sorlei, Phys. Rev. A **64**, 013408 (2001).
[13] G. P. Djotyan, N. Sandor, J. S. Bakos, and Z. Sorlei, J. Opt. Soc. Am. B **26**, 1959 (2009).
[14] M. A. Nielsen and I. L. Chuang, *Quantum Computation and Quantum Information*, 2nd ed. (Cambridge University Press, Cambridge, 2010).
[15] P. Kok and B. W. Lovett, *Introduction to Optical Quantum Information Processing* (Cambridge University Press, Cambridge, 2010).
[16] B. Schumacher and M. Westmoreland, *Quantum Processes, Systems, and Information* (Cambridge University Press, Cambridge, 2010).
[17] S. Kienle, M. Freyberger, W. Schleich, and M. Raymer, in *Experimental Metaphysics: Quantum Mechanical Studies for Abner Shimony*, edited by R. Cohen *et al.* (Kluwer, Lancaster, 1997), pp. 121–133.
[18] M. Freyberger, A. Herkommer, D. Krahmer, E. Mayr, and W. P. Schleich, Adv. At., Mol., Opt. Phys. **41**, 143 (1999).
[19] P. Storey, M. Collett, and D. Walls, Phys. Rev. Lett. **68**, 472 (1992).
[20] P. Storey, M. Collett, and D. Walls, Phys. Rev. A **47**, 405 (1993).
[21] S. Kunze, K. Dieckmann, and G. Rempe, Phys. Rev. Lett. **78**, 2038 (1997).
[22] F. LeKien, G. Rempe, W. P. Schleich, and M. S. Zubairy, Phys. Rev. A **56**, 2972 (1997).
[23] A. M. Herkommer, W. P. Schleich, and M. S. Zubairy, J. Mod. Opt. **44**, 2507 (1997).
[24] E. Paspalakis and P. L. Knight, Phys. Rev. A **63**, 065802 (2001).
[25] M. Sahrai, H. Tajalli, K. T. Kapale, and M. S. Zubairy, Phys. Rev. A **72**, 013820 (2005); K. T. Kapale and M. S. Zubairy, *ibid.* **73**, 023813 (2006).
[26] G. S. Agarwal and K. T. Kapale, J. Phys. B **39**, 3437 (2006).
[27] J. Evers, S. Qamar, and M. S. Zubairy, Phys. Rev. A **75**, 053809 (2007).
[28] G. Yu. Kryuchkyan, M. Macovei, and C. H. Keitel, Phys. Rev. A **77**, 035603 (2008).
[29] M. Macovei, G. Yu. Kryuchkyan, and G.-X. Li, in *Modern Optics and Photonics: Atoms and Structured Media*, edited by G. Yu. Kryuchkyan, G. G. Gurzadyan, and A. V. Papoyan (World Scientific, Singapore, 2010), pp. 32–48.
[30] G. A. Abovyan and G. Yu. Kryuchkyan, J. Phys. B **44**, 045502 (2011).